Commun Nonlinear Sci Numer Simulat 36 (2016) 45–57

Contents lists available at ScienceDirect

Commun Nonlinear Sci Numer Simulat

journal homepage: www.elsevier.com/locate/cnsns

Dynamics and stability of stationary states for the spin-1 Bose–Einstein condensates in a standing light wave

Deng-Shan Wang [a,b,*], Wei Han [c], Yuren Shi [d], Zaidong Li [e], Wu-Ming Liu [f]

[a] School of Science, Beijing Information Science and Technology University, Beijing 100192, PR China
[b] Department of Systems Science, Business School, University of Shanghai for Science and Technology, Shanghai 200093, PR China
[c] Key Laboratory of Time and Frequency Primary Standards, National Time Service Center, Chinese Academy of Sciences, Xi'an 710600, PR China
[d] College of Physics and Electronic Engineering, Northwest Normal University, Lanzhou 730070, PR China
[e] Department of Applied Physics, Hebei University of Technology, Tianjin 300401, PR China
[f] Beijing National Laboratory for Condensed Matter Physics, Institute of Physics, Chinese Academy of Sciences, Beijing 100190, PR China

ARTICLE INFO

Article history:
Received 26 February 2015
Revised 25 September 2015
Accepted 20 November 2015
Available online 2 December 2015

Keywords:
Spin-1 Bose–Einstein condensates
Gross–Pitaevskii equations
Stationary solutions
Linear stability
Dynamical stability

ABSTRACT

The spin-1 Bose–Einstein condensates trapped in a standing light wave can be described by three coupled Gross–Pitaevskii equations with a periodic potential. In this paper, nine families of stationary solutions without phase structures in the form of Jacobi elliptic functions are proposed, and their stabilities are analyzed by both linear stability analysis and dynamical evolutions. Taking the ferromagnetic ^{87}Rb atoms and antiferromagnetic (polar) ^{23}Na atoms as examples, we investigate the stability regions of the nine stationary solutions, which are given in term of elliptic modulus k. It is shown that for the same stationary solution the stability regions of condensates with antiferromagnetic (polar) spin-dependent interactions are larger than that of the condensates with ferromagnetic ones. The dn-dn-dn stationary solution is the most stable solution among the nine families of stationary solutions. Moreover, in the same standing light wave, the spin-1 Bose–Einstein condensates are more stable than the scalar Bose–Einstein condensate.

1. Introduction

The experimental realization of spinor condensates [1,2] opened the possibility to observe various phenomena which are not seen in a single-component Bose–Einstein condensate (BEC). Spinor condensates are distinguished by an additional internal degree of freedom represented by the spin of the atoms. In the case of spin-1 BECs, the dynamics is described by three spin degrees of freedom with $m_F = 1, 0, -1$ of the $F = 1$ atomic hyperfine state. Theoretically, the spin-1 BECs were first studied by Ho [3] through generalizing the three coupled Gross–Pitaevskii (GP) equations under the restriction of gauge and spin-rotation symmetry. Moreover, within the mean-field theory, Ho [3] and Ohmi and Machida [4] predicted a rich set of novel phenomena such as spin textures and topological excitations. Recent years, much work [5–11] has focused on the soliton solutions, dynamics and novel quantum states of spin-1 BECs.

Most BEC experiments use the harmonic confinement, but it is known that BEC loaded into optical lattices shows a wide range of interesting physical properties and complex nonlinear dynamics. Optical lattices [12–17] can be employed to investigate many important physical phenomena of atomic physics and have attracted much attention. A large diversity of remarkable effects in

* Corresponding author. Tel.: +86 1082426014.
E-mail address: dswang@bistu.edu.cn (D.-S. Wang).

http://dx.doi.org/10.1016/j.cnsns.2015.11.018
1007-5704/

optical lattices has already been observed experimentally. Among them we stress on the Bloch oscillations of BECs [18], instability of nonlinear matter waves [19], Landau–Zener tunneling [20], superfluid to Mott-insulator phase transition [21] and gap matter solitons [22]. Carr et al. studied the one dimensional (1D) BEC in quasi-1D confinement in a standing light wave by using the periodic potential $V(x) = -V_0\mathrm{sn}^2(x,k)$ where $\mathrm{sn}(x,k)$ denotes the Jacobian elliptic sine function [23] with elliptic modulus $0 \le k \le 1$, and presented a family of exact stationary solutions to the corresponding GP equation, which is actually a cubic nonlinear Schrödinger equation with an elliptic function potential. Subsequently, researchers [23–26] obtained many exact solutions of other one-component BEC systems and multi-component BEC systems [27–30] in periodic potentials. However, up to now there are few studies on the exact stationary solutions of the spin-1 BECs in periodic potentials.

In this paper, we consider the dynamics and stability of stationary states for BECs of alkali atoms in the $F = 1$ hyperfine states confined in a standing light wave [23]. In the framework of mean-field theory, the dynamics of the spinor condensates is described by the three component GP equations with periodic potential as

$$i\frac{\partial\Psi_0}{\partial t} = [\mathcal{H}_0 + c_2(|\Psi_{+1}|^2 + |\Psi_{-1}|^2)]\Psi_0 + 2c_2\Psi_0^*\Psi_{+1}\Psi_{-1}, \tag{1a}$$

$$i\frac{\partial\Psi_{\pm1}}{\partial t} = [\mathcal{H}_0 + c_2(|\Psi_{\pm1}|^2 + |\Psi_0|^2 - |\Psi_{\mp1}|^2)]\Psi_{\pm1} + c_2\Psi_{\mp1}^*\Psi_0^2, \tag{1b}$$

where $\mathcal{H}_0 = -\frac{1}{2}\nabla^2 + V(\mathbf{r}) + c_0(|\Psi_{-1}|^2 + |\Psi_0|^2 + |\Psi_{+1}|^2)$ and the external potential $V(\mathbf{r}) = \frac{1}{2}\omega_\perp^2(y^2+z^2) + V_{\mathrm{OL}}(x)$, with $\omega_\perp$ being the trapping frequency in the direction perpendicular to the lattice. The function $V_{\mathrm{OL}}(x) = V_0\mathrm{sn}^2(dx,k)$ is a periodic potential, where V_0 is the depth of the optical lattice, d is the wave number of the laser lights that generate the optical lattice and k is the elliptic modulus with $0 \le k \le 1$. Note that when $k = 0$ the 1D potential is sinusoidal and thus $V_{\mathrm{OL}}(x) = V_0\sin^2(dx)$ is exactly a standing light wave. For most intermediate values of k (e.g. $0 < k < 0.9$) the potential is virtually indistinguishable from a sinusoidal potential and thus can be well approximated by the standing light wave potential generated experimentally. For the case $k \to 1^-$, the 1D optical lattice becomes an array of well separated hyperbolic secant potential barriers or wells. Any elliptic function $\mathrm{sn}(dx,k)$ can be expanded as infinite series of trigonometric functions by the well known formula [31]

$$\mathrm{sn}(dx,k) = \frac{2\pi}{kK(k^2)}\sum_{n=0}^{\infty}\frac{q^{n+1/2}}{1-q^{2n+1}}\sin\frac{(2n+1)\pi dx}{2K(k^2)},$$

where $q = \exp\{-\pi[K(1-k^2)/K(k^2)]\}$ and $K(k^2)$ is a complete elliptic integral of the first kind [31]. From this formula, one can find that even for relatively large elliptic modulus, such as $k_0^2 = 0.9$, one obtains $q \approx 0.084$ which means that

$$\mathrm{sn}(dx,k) \approx \frac{2\pi^2 q}{k^2K^2(k^2)(1-q)^2}\left[1 - \cos\frac{\pi dx}{K(k^2)} + \frac{2q}{1+q+q^2}\left(\cos\frac{\pi dx}{K(k^2)} - \cos\frac{2\pi dx}{K(k^2)}\right)\right],$$

for $k < k_0$. This potential can be produced by using only two laser beams, and the elliptic function potential $\mathrm{sn}(dx,k)$ is approximated with accuracy higher than 99%. The accuracy of the approximation increases as k decreases. Anyway, for most values of k, the elliptic function potential $\mathrm{sn}^2(dx,k)$ can be well approximated by only a few laser beams in real experiments [29,30].

The wave functions Eq. (1) are normalized to the number of atoms as $\int|\Psi_j|^2 d\mathbf{r} = N_j$, where $j = \pm1, 0$, and $\mathcal{N} = N_1 + N_2 + N_3$ is the total number of atoms in the condensate. The units for length, time and energy are $a_\perp = (\hbar/M\omega_\perp)^{1/2}$, $\omega_\perp^{-1}$ and $\hbar\omega_\perp$, respectively. Moreover, the parameters c_0 and c_2 describing binary elastic collisions of spin-1 atoms in the combined symmetric channel of total spin 0 and 2, are expressed as $c_0 = 2(a_0 + 2a_2)/(3a_\perp)$ and $c_2 = 2(a_2 - a_0)/(3a_\perp)$ with a_0, a_2 being the s-wave scattering lengths. Note that the $F = 1$ spinor condensates may be either ferromagnetic (such as the ^{87}Rb atoms), characterized by $c_2 < 0$ [32], or polar (such as the ^{23}Na atoms), with $c_2 > 0$ [33]. For ^{87}Rb atoms [32], the scattering lengths $a_0 = 101.8a_B$ and $a_2 = 100.4a_B$ (a_B is Bohr radius) are nearly equal, and the dimensionless 1D coupling constants are $c_0 = 1.49\times10^{-2}$ and $c_2 = -6.94\times10^{-5}$, indicating that the spin-dependent mean-field energy c_2n, are very small for density n compared with both the scalar mean field c_0n. For ^{23}Na atoms [33], the scattering lengths are $a_0 = 50a_B$ and $a_2 = 55a_B$, and the dimensionless 1D coupling constants are $c_0 = 4.08\times10^{-3}$ and $c_2 = 1.28\times10^{-4}$.

In the limit of highly elongated traps, the tight confinement ensures that no excited states are available in the transverse direction and thus the dynamics takes place along the axial direction. By introducing separable wave functions $\Psi_j(\mathbf{r}) = \psi_j(x,t)\psi_\perp(y,z)$ with the transverse components $\psi_\perp(y,z)$ determined by the ground state of the tight harmonic trap, and integrating 3D GP equations (1) over the transverse directions $\{y,z\}$, the model for the spinor condensate is reduced to the quasi-one-dimensional three-component GP equations for $\psi_j(x)$ as

$$i\frac{\partial\psi_0}{\partial t} = [\mathcal{L} + c_2(|\psi_{+1}|^2 + |\psi_{-1}|^2)]\psi_0 + 2c_2\psi_0^*\psi_{+1}\psi_{-1}, \tag{2a}$$

$$i\frac{\partial\psi_{\pm1}}{\partial t} = [\mathcal{L} + c_2(|\psi_{\pm1}|^2 + |\psi_0|^2 - |\psi_{\mp1}|^2)]\psi_{\pm1} + c_2\psi_{\mp1}^*\psi_0^2, \tag{2b}$$

where $\mathcal{L} = -\frac{1}{2}\frac{\partial^2}{\partial x^2} + V_0\mathrm{sn}^2(dx,k) + c_0(|\psi_{-1}|^2 + |\psi_0|^2 + |\psi_{+1}|^2)$.

2. Stationary solutions and linear stability analysis

2.1. Exact stationary solutions of three-component GP equations

In this subsection, we present the stationary solutions of the quasi-one-dimensional three-component GP equations (2) in closed form and study their stabilities numerically. For simplicity, we fix the parameter $d = 1$ in the 1D periodic potential. We begin by constructing stationary solutions with trivial phase to Eq. (2) in the following forms

$$\psi_m = \phi_m \exp[i(k_m t + \omega_m)], \quad m = +1, 0, -1, \tag{3}$$

where ϕ_m are real functions of x, and parameters k_m and ω_m are constants.

Substituting (3) in (2) and setting parameters $k_0 = k_1/2 + k_{-1}/2$ and $\omega_0 = \omega_{-1}/2 + \omega_1/2$, we obtain the following three stationary equations of ϕ_1, ϕ_0 and ϕ_{-1} as

$$\mathcal{L}_1\phi_1 = n_0\phi_1 + c_2\left(\phi_1^3 - \phi_{-1}^2\phi_1 + \phi_1\phi_0^2 + \phi_{-1}\phi_0^2\right), \tag{4a}$$

$$\mathcal{L}_0\phi_0 = n_0\phi_0 + c_2\left(2\,\phi_0\phi_1\phi_{-1} + \phi_0\phi_1^2 + \phi_0\phi_{-1}^2\right), \tag{4b}$$

$$\mathcal{L}_{-1}\phi_{-1} = n_0\phi_{-1} + c_2\left(\phi_{-1}^3 - \phi_1^2\phi_{-1} + \phi_{-1}\phi_0^2 + \phi_1\phi_0^2\right), \tag{4c}$$

where $\mathcal{L}_1 = \frac{1}{2}\frac{\partial^2}{\partial x^2} - V_0\mathrm{sn}^2(x,k) + n_0 - k_1$, $\mathcal{L}_{-1} = \frac{1}{2}\frac{\partial^2}{\partial x^2} - V_0\mathrm{sn}^2(x,k) + n_0 - k_{-1}$, $\mathcal{L}_0 = \frac{1}{2}\frac{\partial^2}{\partial x^2} - V_0\mathrm{sn}^2(x,k) + n_0 - (k_1 + k_{-1})/2$ and $n_0 = \phi_{-1}^2 + \phi_0^2 + \phi_1^2$.

Based on the approach in [23], we obtain nine closed form solutions for the stationary equations (4), and then get nine families of exact solutions of the three-component GP Eq. (2) as follows:

Solution 1. If $k^2 - 2\,c_0{a_1}^2 - V_0 > 0$, we have

$$\psi_1 = a_1\mathrm{sn}(x,k)\mathrm{e}^{-i[(1+k^2)t - 2\,\omega_1]/2}, \tag{5a}$$

$$\psi_0 = \sqrt{(k^2 - 2\,c_0{a_1}^2 - V_0)/c_0}\,\mathrm{sn}(x,k)\mathrm{e}^{i[\omega_0 - (\frac{1}{2} + \frac{k^2}{2})t]}, \tag{5b}$$

$$\psi_{-1} = -a_1\mathrm{sn}(x,k)\mathrm{e}^{-i[(1+k^2)t - 2\,\omega_{-1}]/2}. \tag{5c}$$

Solution 2. If $V_0 - k^2 - 2\,c_0{a_1}^2 > 0$, we have

$$\psi_1 = a_1\mathrm{cn}(x,k)\mathrm{e}^{i[(2\,k^2 - 1 - 2\,V_0)t + 2\,\omega_1]/2}, \tag{6a}$$

$$\psi_0 = \sqrt{(V_0 - k^2 - 2\,c_0{a_1}^2)/c_0}\,\mathrm{cn}(x,k)\mathrm{e}^{i[(k^2 - \frac{1}{2} - V_0)t + \omega_0]}, \tag{6b}$$

$$\psi_{-1} = -a_1\mathrm{cn}(x,k)\mathrm{e}^{i[(2\,k^2 - 1 - 2\,V_0)t + 2\,\omega_{-1}]/2}. \tag{6c}$$

Solution 3. If $V_0 - k^2 - 2\,c_0{a_1}^2k^2 > 0$, we have

$$\psi_1 = a_1\mathrm{dn}(x,k)\mathrm{e}^{i[(2 - k^2 - 2\,V_0/k^2)t + 2\,\omega_1]/2}, \tag{7a}$$

$$\psi_0 = \frac{\sqrt{(V_0 - k^2 - 2\,c_0{a_1}^2k^2)/c_0}}{k}\mathrm{dn}(x,k)\mathrm{e}^{i[(1 - \frac{k^2}{2} - \frac{V_0}{k^2})t + \omega_0]}, \tag{7b}$$

$$\psi_{-1} = -a_1\mathrm{dn}(x,k)\mathrm{e}^{i[(2 - k^2 - 2\,V_0/k^2)t + 2\,\omega_{-1}]/2}. \tag{7c}$$

Solution 4. If $c_2 > 0$ and $V_0 = \frac{k^2(c_2 - c_0)}{2c_2}$, we have

$$\psi_1 = \frac{-\gamma_1}{2c_2}\mathrm{sn}(x,k)e^{-\frac{i}{2}[(1+k^2)t + \gamma_{2+}a_1t + 4\,c_0a_1^2t - 2\,\omega_1]}, \tag{8a}$$

$$\psi_0 = \frac{\sqrt{c_2a_1\gamma_1}}{c_2}\mathrm{cn}(x,k)\mathrm{e}^{i[\omega_0 - (2\,c_0{a_1}^2 + \frac{\sqrt{2}c_0a_1k}{\sqrt{c_2}} + \frac{1}{2})t]}, \tag{8b}$$

$$\psi_{-1} = a_1\mathrm{sn}(x,k)e^{\frac{i}{2}[(k^2-1)t + \gamma_{2-}a_1t - 4\,c_0a_1^2t + 2\,\omega_{-1}]}, \tag{8c}$$

where $\gamma_1 = 2\,c_2a_1 + \sqrt{2c_2}k$ and $\gamma_{2\pm} = 2\sqrt{2c_2}k \pm \frac{2\sqrt{2}c_0k}{\sqrt{c_2}}$.

Solution 5. If $c_2 > 0$ and $V_0 = \frac{k^2(c_2 - c_0)}{2c_2}$, we have

$$\psi_1 = a_1\mathrm{sn}(x,k)e^{\frac{i}{2}[(1-k^2)t + \frac{2\sqrt{2}(c_2 - c_0)a_1t}{\sqrt{c_2}k} - \frac{4a_1{}^2c_0t}{k^2} + 2\,\omega_1]}, \tag{9a}$$

$$\psi_0 = \frac{\sqrt{c_2a_1\gamma_3}}{c_2k}\mathrm{dn}(x,k)\mathrm{e}^{i[\omega_0 - (\frac{2c_0a_1^2}{k^2} + \frac{\sqrt{2}a_1c_0}{k\sqrt{c_2}} + \frac{k^2}{2})t]}, \tag{9b}$$

$$\psi_{-1} = -\frac{\gamma_3}{2c_2}\mathrm{sn}(x,k)e^{\frac{i}{2}[2\,\omega_{-1} - (1+k^2)t - \frac{2\sqrt{2}(c_2 + c_0)a_1t}{\sqrt{c_2}k} - \frac{4a_1{}^2c_0t}{k^2}]}, \tag{9c}$$

where $\gamma_3 = 2\,c_2a_1 + \sqrt{2c_2}k$.

Solution 6. If $c_2 < 0$ and $V_0 = \frac{k^2(c_2-c_0)}{2c_2}$, we have

$$\psi_1 = a_1 \mathrm{cn}(x,k) e^{-\frac{i}{2}[(1-\frac{c_0k^2}{c_2}+k^2)t+\gamma_{5-}t+4a_1^2c_0t-2\omega_1]}, \tag{10a}$$

$$\psi_0 = \frac{\sqrt{c_2a_1\gamma_4}}{c_2}\mathrm{sn}(x,k)\mathrm{e}^{i[(\frac{c_0k^2}{2c_2}-2c_0a_1{}^2-\frac{a_1c_0k\sqrt{-2c_2}}{c_2}-\frac{1}{2})t+\omega_0]}, \tag{10b}$$

$$\psi_{-1} = -\frac{\gamma_4}{2c_2}\mathrm{cn}(x,k) e^{-\frac{i}{2}[(1-k^2-\frac{c_0k^2}{c_2})t+\gamma_{5+}t+4a_1{}^2c_0t-2\omega_{-1}]}, \tag{10c}$$

where $\gamma_4 = 2a_1c_2+\sqrt{-2c_2}k$ and $\gamma_{5\pm} = 2k\sqrt{-2c_2}(\frac{c_0}{c_2}\pm 1)a_1$.

Solution 7. If $c_2 < 0$ and $V_0 = \frac{k^2(c_2-c_0)}{2c_2}$, we have

$$\psi_1 = a_1 \mathrm{dn}(x,k) e^{-\frac{i}{2}[(1+k^2-\frac{c_0}{c_2})t+\gamma_{7-}t+4a_1^2c_0t-2\omega_1]}, \tag{11a}$$

$$\psi_0 = \frac{\sqrt{\sqrt{-2c_2}a_1\gamma_6 k}}{\sqrt{-c_2}}\mathrm{sn}(x,k)\mathrm{e}^{i[(\frac{c_0}{2c_2}-2c_0a_1^2-\frac{a_1\sqrt{-2c_2}c_0}{c_2}-\frac{k^2}{2})t+\omega_0]}, \tag{11b}$$

$$\psi_{-1} = \frac{\sqrt{-2c_2}\gamma_6}{2c_2}\mathrm{dn}(x,k) e^{-\frac{i}{2}[(k^2-\frac{c_0}{c_2}-1)t+\gamma_{7+}t+4a_1^2c_0t-2\omega_{-1}]}, \tag{11c}$$

where $\gamma_6 = a_1\sqrt{-2c_2}-1$ and $\gamma_{7\pm} = \frac{2\sqrt{-2c_2}a_1}{c_2}(c_0\pm c_2)$.

Solution 8. If $c_2 < 0$ and $V_0 = \frac{k^2(c_2-c_0)}{2c_2}$, we have

$$\psi_1 = a_1 \mathrm{dn}(x,k) e^{\frac{i}{2}[\gamma_{9+}t+4c_0(k^2-1)a_1{}^2t+2\omega_1]}, \tag{12a}$$

$$\psi_0 = \tilde{a}_0 \mathrm{cn}(x,k)\mathrm{e}^{i\{[a_1c_0(k^2-1)(2a_1-\frac{\sqrt{-2c_2}}{c_2})+\frac{c_0}{2c_2}]t+\omega_0\}}, \tag{12b}$$

$$\psi_{-1} = \frac{\sqrt{-2c_2}\gamma_8}{2c_2}\mathrm{dn}(x,k) e^{-\frac{i}{2}[\gamma_{9-}t-4c_0(k^2-1)a_1^2t-2\omega_{-1}]}, \tag{12c}$$

where $\gamma_8 = a_1\sqrt{-2c_2}+1$, $\tilde{a}_0 = \frac{\sqrt{-2\sqrt{-2c_2}a_1\gamma_8 k}}{\sqrt{-2c_2}}$ and $\gamma_{9\pm} = \frac{k^2c_2\pm c_0-c_2}{c_2} + \frac{2\sqrt{-2c_2}(k^2-1)(c_2\mp c_0)a_1}{c_2}$.

Solution 9. If $c_2 < 0$ and $V_0 = \frac{k^2(c_2-c_0)}{2c_2}$, we have

$$\psi_1 = a_1 \mathrm{cn}(x,k) e^{\frac{i}{2}[\gamma_{12-}t-\frac{4c_0(k^2-1)a_1^2t}{k^2}+2\omega_1]}, \tag{13a}$$

$$\psi_0 = \frac{\sqrt{c_2\gamma_{10}a_1}}{c_2k}\mathrm{dn}(x,k)\mathrm{e}^{i[(\gamma_{11}-\frac{a_1\sqrt{-2c_2}c_0}{c_2k}-\frac{2c_0a_1{}^2(k^2-1)}{k^2})t+\omega_0]}, \tag{13b}$$

$$\psi_{-1} = \frac{\gamma_{10}}{2c_2}\mathrm{cn}(x,k) e^{\frac{i}{2}[\gamma_{12+}t-\frac{4c_0(k^2-1)a_1^2t}{k^2}+2\omega_{-1}]}. \tag{13c}$$

where $\gamma_{10} = k\sqrt{-2c_2}-2c_2a_1$, $\gamma_{11} = \frac{c_0k(2a_1\sqrt{-2c_2}+k)}{2c_2}$ and $\gamma_{12\pm} = \frac{k^2c_0\pm k^2c_2\mp c_2}{c_2} \pm \frac{2\sqrt{-2c_2}(k^2-1)(c_2\pm c_0)a_1}{c_2k}$.

2.2. Linear stability analysis

In the above subsection, nine families of stationary solutions to the governing Eq. (2) have been found. It is known that only solutions that are stable can be observed in real experiments. Thus it is important to investigate the stability regions of these stationary solutions. In this subsection, we first consider the linear stability of the nine families of stationary solutions. To do so, we consider an infinitesimally small perturbation [23] of the exact solution as

$$\psi_m = (\phi_m(x)+\varphi_m(x,t))\exp[i(k_mt+\omega_m)], m = 0, \pm 1, \tag{14}$$

where $\phi_m(x)\exp[i(k_mt+\omega_m)]$ is the stationary solution presented previously and $\varphi_m(x,t) \ll 1$ is a small perturbation to the exact solution. Decomposing perturbation term $\varphi_m(x,t)$ into real and imaginary parts as $\varphi_m(x,t) = U_m(x,t)+iV_m(x,t)$ and substituting (14) into (2), we have

$$\frac{d\mathcal{V}}{dt} = \mathcal{M}\mathcal{V}, \tag{15}$$

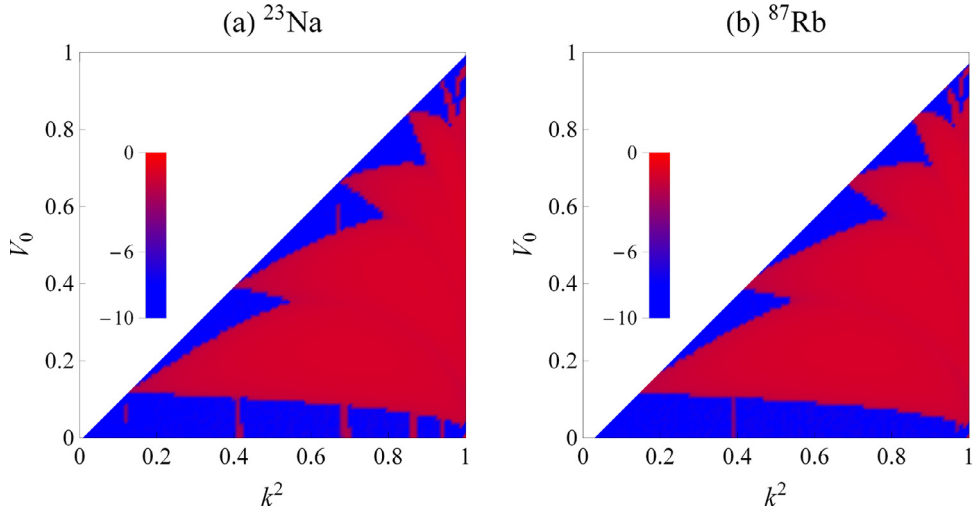

Fig. 1. Linear stability phase diagrams as functions of the depth of optical lattice V_0 and the square of elliptic modulus k^2 for the stationary solution 1 in Eq. (5) with parameters $\omega_1 = \omega_0 = \omega_{-1} = 0$ and $a_1 = 1$. The left plot is for ^{23}Na condensates and the right one is for ^{87}Rb atom, where we have taken the logarithm for eigenvalue λ. The blue color stands for linear stability region and the red color stands for linear instability region. (For interpretation of the references to color in this figure legend, the reader is referred to the web version of this article).

where $\mathcal{V} = (U_1, V_1, U_0, V_0, U_{-1}, V_{-1})'$ with $'$ denoting transpose and matrix $\mathcal{M}$ is

$$\mathcal{M} = \begin{pmatrix} 0 & T+L_1 & 0 & K_1 & 0 & K_2 \\ -T-L_2 & 0 & M_1 & 0 & M_2 & 0 \\ 0 & K_1 & 0 & T+L_3 & 0 & K_3 \\ M_1 & 0 & -T-L_4 & 0 & M_3 & 0 \\ 0 & K_2 & 0 & K_3 & 0 & T+L_5 \\ M_2 & 0 & M_3 & 0 & -T-L_6 & 0 \end{pmatrix}$$

with $T = -\frac{1}{2}\partial_x^2$, $K_1 = 2c_2\phi_{-1}\phi_0$, $K_2 = -c_2{\phi_0}^2$, $K_3 = 2c_2\phi_1\phi_0$ and

$$\begin{aligned}
L_1 &= c_0 n_0 + c_2({\phi_1}^2 + {\phi_0}^2 - {\phi_{-1}}^2) + V_0 \mathrm{sn}^2(x,k) + k_1, \\
L_2 &= c_0(n_0 + 2{\phi_1}^2) + c_2(3{\phi_1}^2 + {\phi_0}^2 - {\phi_{-1}}^2) + V_0 \mathrm{sn}^2(x,k) + k_1, \\
L_3 &= c_0 n_0 + c_2(\phi_1 - \phi_{-1})^2 + V_0 \mathrm{sn}^2(x,k) + \frac{1}{2}(k_1 + k_{-1}), \\
L_4 &= c_0(n_0 + 2{\phi_0}^2) + c_2(\phi_1 + \phi_{-1})^2 + V_0 \mathrm{sn}^2(x,k) + \frac{1}{2}(k_1 + k_{-1}), \\
L_5 &= c_0 n_0 + c_2({\phi_0}^2 - {\phi_1}^2 + {\phi_{-1}}^2) + V_0 \mathrm{sn}^2(x,k) + k_{-1}, \\
L_6 &= c_0(n_0 + 2{\phi_{-1}}^2) + c_2({\phi_0}^2 - {\phi_1}^2 + 3{\phi_{-1}}^2) + V_0 \mathrm{sn}^2(x,k) + k_{-1},
\end{aligned}$$

$$\begin{aligned}
M_1 &= -2c_0\phi_1\phi_0 - 2(\phi_1 + \phi_{-1})\phi_0 c_2, \\
M_2 &= -2c_0\phi_1\phi_{-1} + (2\phi_1\phi_{-1} - {\phi_0}^2)c_2, \\
M_3 &= -2c_0\phi_{-1}\phi_0 - 2(\phi_1 + \phi_{-1})\phi_0 c_2.
\end{aligned}$$

Separating the time-space dependent functions $U_1, V_1, U_0, V_0, U_{-1}$ and V_{-1} from the spatial variations as

$$\begin{pmatrix} U_1 \\ V_1 \\ U_0 \\ V_0 \\ U_{-1} \\ V_{-1} \end{pmatrix} = e^{\lambda t} \begin{pmatrix} u_1 \\ v_1 \\ u_0 \\ v_0 \\ u_{-1} \\ v_{-1} \end{pmatrix}, \tag{16}$$

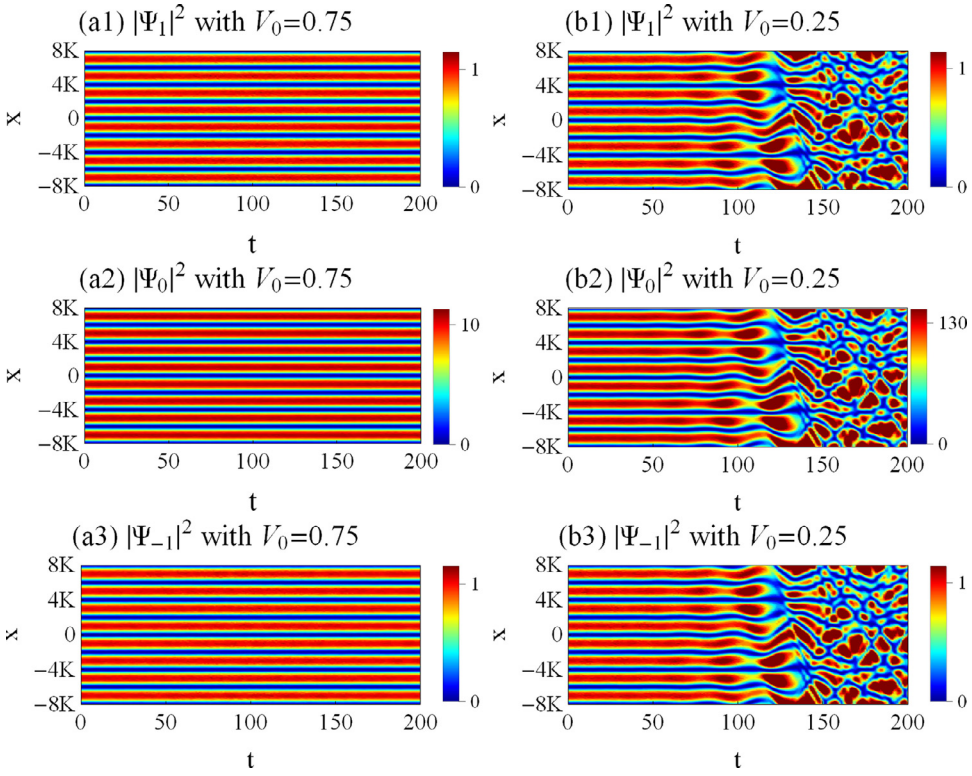

Fig. 2. Dynamical evolutions of the density distributions $|\psi_m|^2$ of the ^{23}Na condensate described by stationary solution 1 in Eq. (5) with $k^2 = 0.8$ and parameter $a_1 = 1, \omega_m = 0 (m = 0, \pm 1)$. The left column denotes the stationary solution 1 is dynamically stable for $V_0 = 0.75$, and the right column denotes it is dynamically unstable for $V_0 = 0.25$, which is consistent with the linear stability analysis in Fig. 1(a).

where $u_1, v_1, u_0, v_0, u_{-1}$ and v_{-1} are functions of x, we get the following eigenvalue problem from Eq. (15)

$$\mathcal{M}\begin{pmatrix} u_1 \\ v_1 \\ u_0 \\ v_0 \\ u_{-1} \\ v_{-1} \end{pmatrix} = \lambda \begin{pmatrix} u_1 \\ v_1 \\ u_0 \\ v_0 \\ u_{-1} \\ v_{-1} \end{pmatrix}. \tag{17}$$

If all eigenvalues λ in Eq. (17) are purely imaginary or only have negative real parts, the exact stationary solutions from (5) to (13) are linearly stable. In contrast, if there is at least one eigenvalue with positive real part, then instability results. The linear stability of the nine stationary solutions from (5) to (13) can be examined by numerically solving the eigenvalue problem (17).

3. Dynamics and Stability

In this section, we examine the dynamics and stability of the nine stationary solutions in Eqs. (5)–(13) of the three-component GP equations (2) numerically. Specifically, we consider the spinor BEC clouds with either ferromagnetic or antiferromagnetic (polar) spin-dependent interactions. It is known that ferromagnetic or antiferromagnetic type of the spinor condensate is dependent on the sign of the coefficient c_2 (c_0 is always positive for condensates with repulsive interactions, such as the ^{23}Na and ^{87}Rb considered here). Thus the dynamics and stability of the nine stationary solutions in Eqs. (5)–(13) should be examined by considering $c_2 < 0$ and $c_2 > 0$, respectively. In the following analysis, we adopt the experimental data of ^{23}Na and ^{87}Rb atoms in Table 1, where the dimensionless 1D coupling constants c_0 is always positive.

3.1. Dynamics and stability of the stationary solutions 1–3

We first analyze the dynamics and stability of the exact stationary solutions 1–3 in Eqs. (5)–(7). In our framework, the dimensionless 1D coupling constants $c_0 > 0$, thus the restriction on stationary solution 1 in Eq. (5) is $k^2 - 2c_0{a_1}^2 - V_0 > 0$, on stationary solution 2 in Eq. (6) is $V_0 - k^2 - 2c_0{a_1}^2 > 0$ and on stationary solution 3 in Eq. (7) is $V_0 - k^2 - 2c_0{a_1}^2k^2 > 0$, where there are no any restrictions on the coupling constants c_2. Thus the exact stationary solutions (5)–(7) exist for any choices of the coupling constants c_2. Note that the stability of these solutions is affected by both the depth V_0 of the optical lattice and the

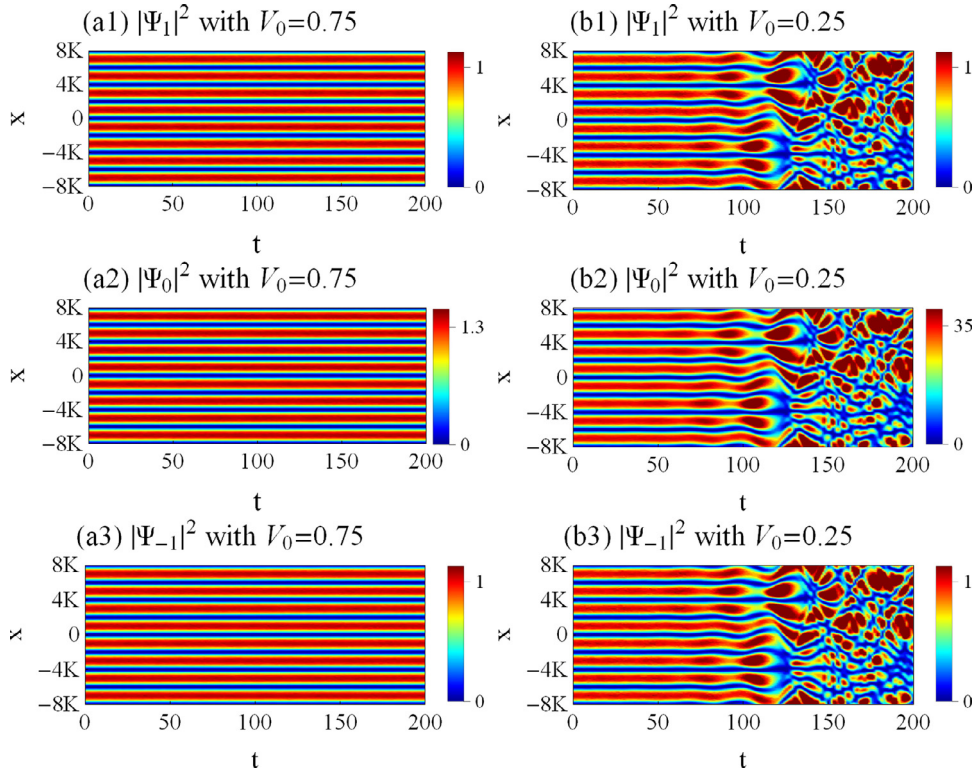

Fig. 3. Dynamical evolutions of the density distributions $|\psi_m|^2$ of the ^{87}Rb condensate described by stationary solution 1 in Eq. (5) with $k^2 = 0.8$ and parameter $a_1 = 1, \omega_m = 0 (m = 0, \pm 1)$. The left column indicates the stationary solution 1 is dynamically stable for $V_0 = 0.75$, and the right column indicates it is dynamically unstable for $V_0 = 0.25$. These are consistent with the linear stability analysis in Fig. 1(b).

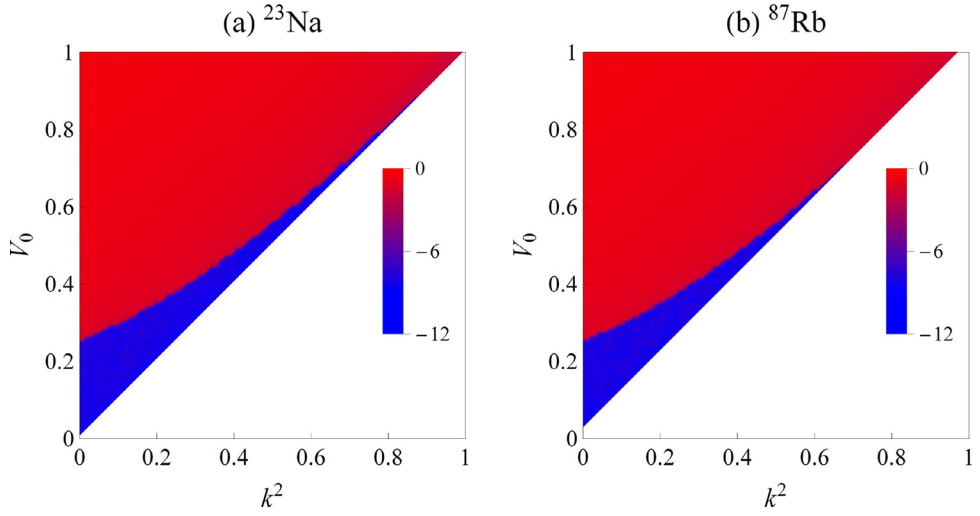

Fig. 4. Linear stability phase diagrams as functions of the depth of optical lattice V_0 and the square of elliptic modulus k^2 for the stationary solution 2 in Eq. (6) with parameters $\omega_1 = \omega_0 = \omega_{-1} = 0$ and $a_1 = 1$. The left is for ^{23}Na and the right is for ^{87}Rb atom, where we have taken the logarithm for eigenvalue λ. The blue color stands for linear stability region and the red color stands for linear instability region. (For interpretation of the references to color in this figure legend, the reader is referred to the web version of this article).

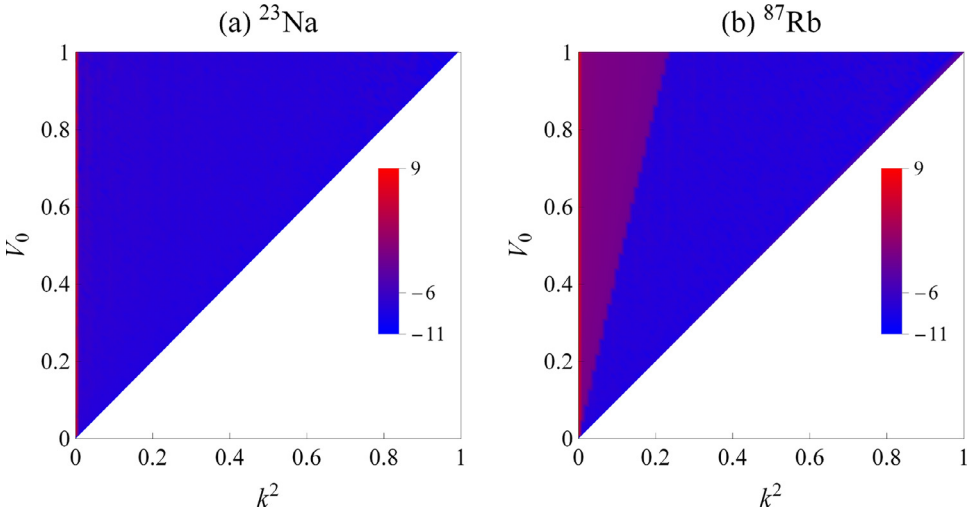

Fig. 5. Linear stability phase diagrams as functions of the depth of optical lattice V_0 and the square of elliptic modulus k^2 for the stationary solution 3 in Eq. (7) with parameters $\omega_1 = \omega_0 = \omega_{-1} = 0$ and $a_1 = 1$. The left is for ^{23}Na and the right is for ^{87}Rb atom, where we have taken the logarithm for eigenvalue λ. The blue stands for linear stability region and the purple stands for weak linear stability region. (For interpretation of the references to color in this figure legend, the reader is referred to the web version of this article).

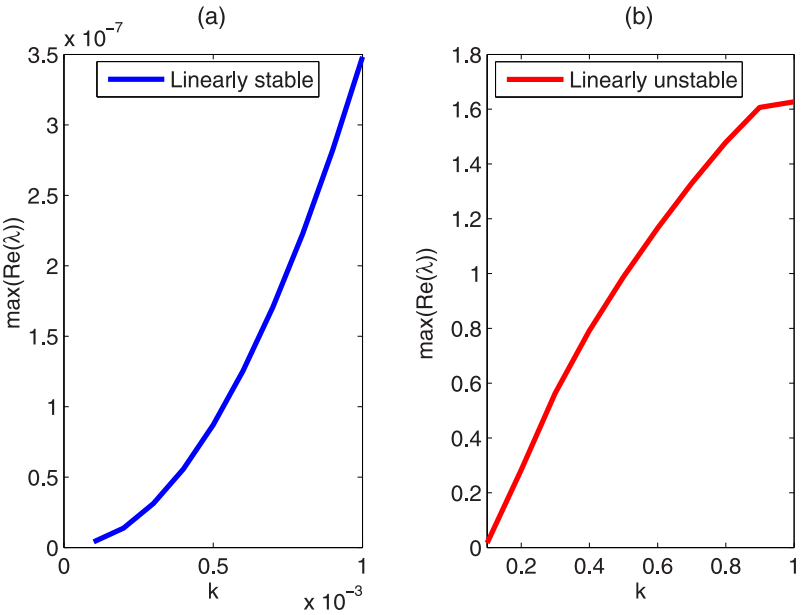

Fig. 6. Real parts of maximal linear eigenvalues versus the elliptic modulus k for the stationary solutions 4 in Eq. (8) with parameters $a_1 = 1, \omega_m = 0 (m = 0, \pm 1)$ and the spin-dependent interaction parameters c_0, c_2 for ^{23}Na atoms.

Table 1
Experimental data of scattering lengths a_0, a_2 given in units of the Bohr radius a_B, and the dimensionless 1D coupling constants c_0 and c_2 for ^{23}Na and ^{87}Rb atoms, respectively.

	a_0	a_2	c_0	c_2
^{23}Na	$50a_B$	$55a_B$	4.08×10^{-3}	1.28×10^{-4}
^{87}Rb	$101.8a_B$	$100.4a_B$	1.49×10^{-2}	-6.94×10^{-5}

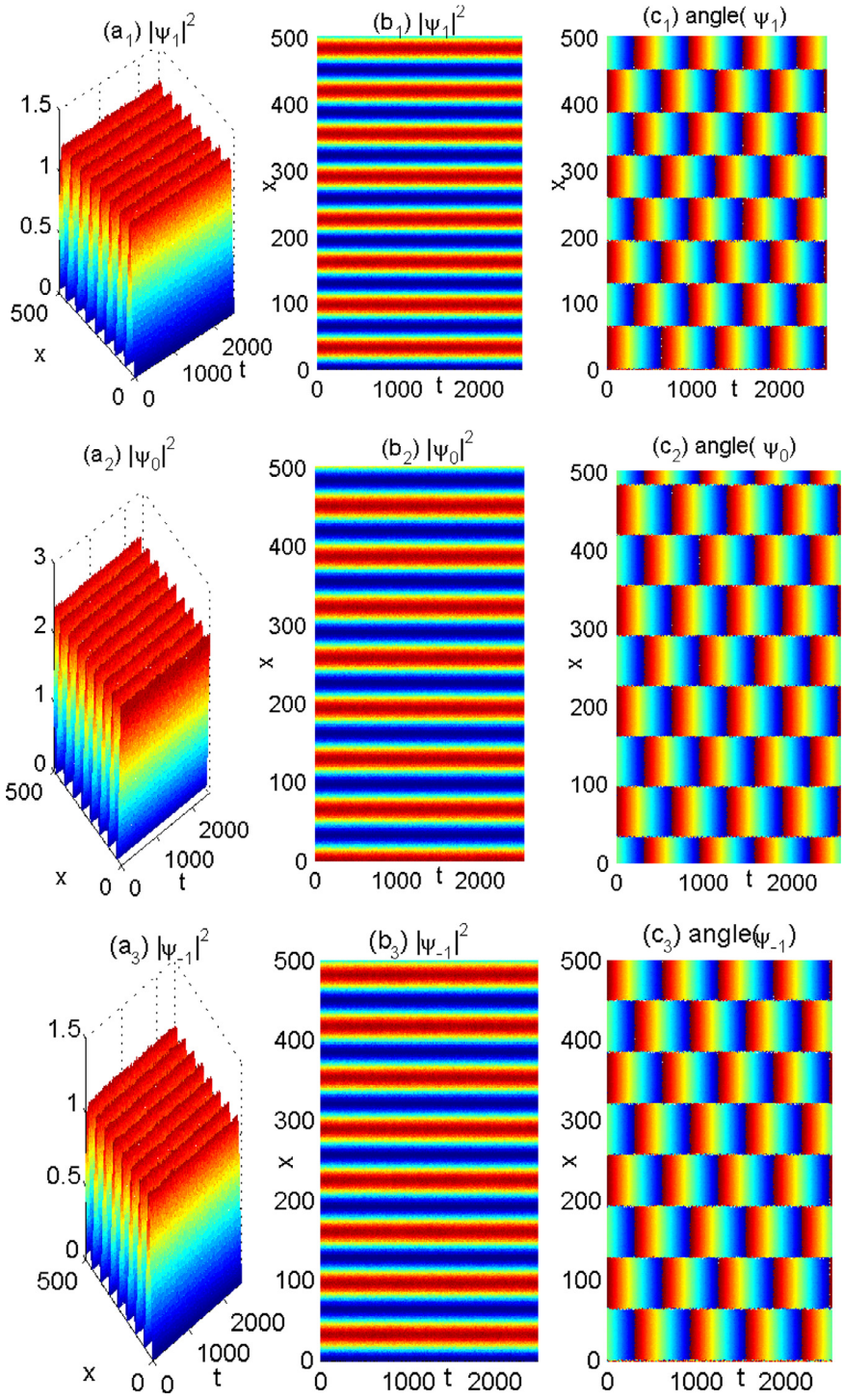

Fig. 7. Dynamical evolutions of the density distributions and phases of the ^{23}Na condensate described by stationary solution 4 in Eq. (8) with elliptic modulus $k = 0.001$ and parameter $a_1 = 1, \omega_m = 0 (m = 0, \pm 1)$.

elliptic modulus k in the solutions. Thus we need to study the phase diagrams of V_0 and k to reveal the linear stability regions by solving the eigenvalue problem (17) numerically. From Eq. (16) it is seen that the stationary solutions are linearly stable if all the real parts of eigenvalues λ are non-positive.

In Fig. 1, numerical experiments demonstrate the linear stability phase diagrams as functions of the depth of optical lattice V_0 and the square of elliptic modulus k^2 for solution 1 in Eq. (5) with parameter $a_1 = 1$ and $\omega_1 = \omega_0 = \omega_{-1} = 0$ for ^{23}Na and ^{87}Rb atoms, respectively. Here and in Figs. 4 and 5, we have taken the logarithm for eigenvalue λ. The blue region corresponds

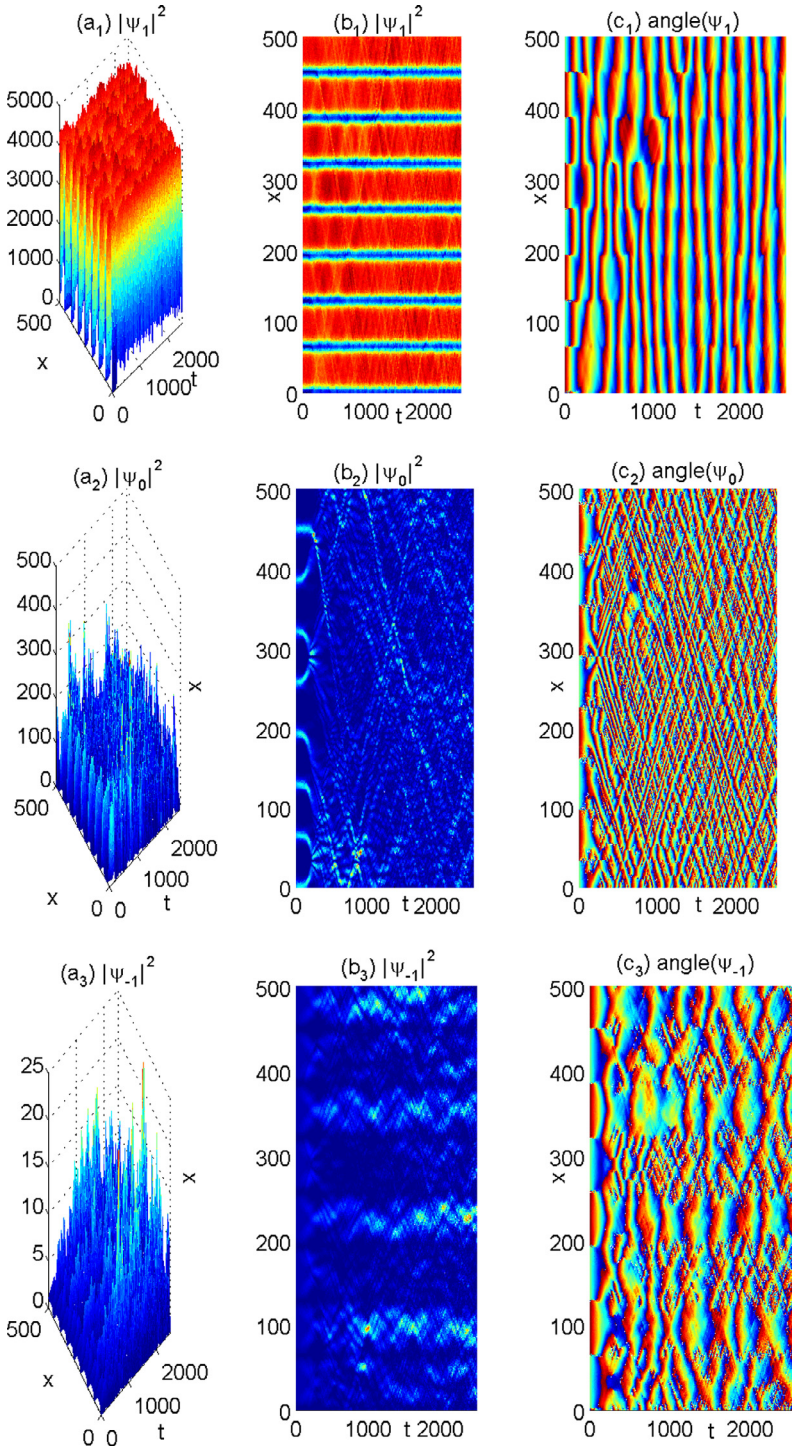

Fig. 8. Dynamical evolutions of the density distributions and phases of the ^{23}Na condensate described by stationary solution 4 in Eq. (8) with elliptic modulus $k = 0.999$ and parameter $a_1 = 1, \omega_m = 0 (m = 0, \pm 1)$.

eigenvalue λ approaching to zero, which is the linear stability region, and the red region is the linear instability region. Fig. 2 shows the dynamics of the density distributions $|\psi_m|^2$ of the ^{23}Na condensate described by stationary solution 1 in Eq. (5) with elliptic modulus $k^2 = 0.8$ and the parameters in Fig. 1(a). It is seen that the stationary solution 1 is dynamically unstable for the depth of optical lattice $V_0 = 0.25$ (the right column), and it is dynamically stable for $V_0 = 0.75$ (the left column), which is consistent with the linear stability analysis in Fig. 1(a). Fig. 3 shows the dynamics of the density distributions $|\psi_m|^2$ of the ^{87}Rb condensate described by stationary solution 1 in Eq. (5) with elliptic modulus $k^2 = 0.8$ and the parameters in Fig. 1(b). For ^{87}Rb

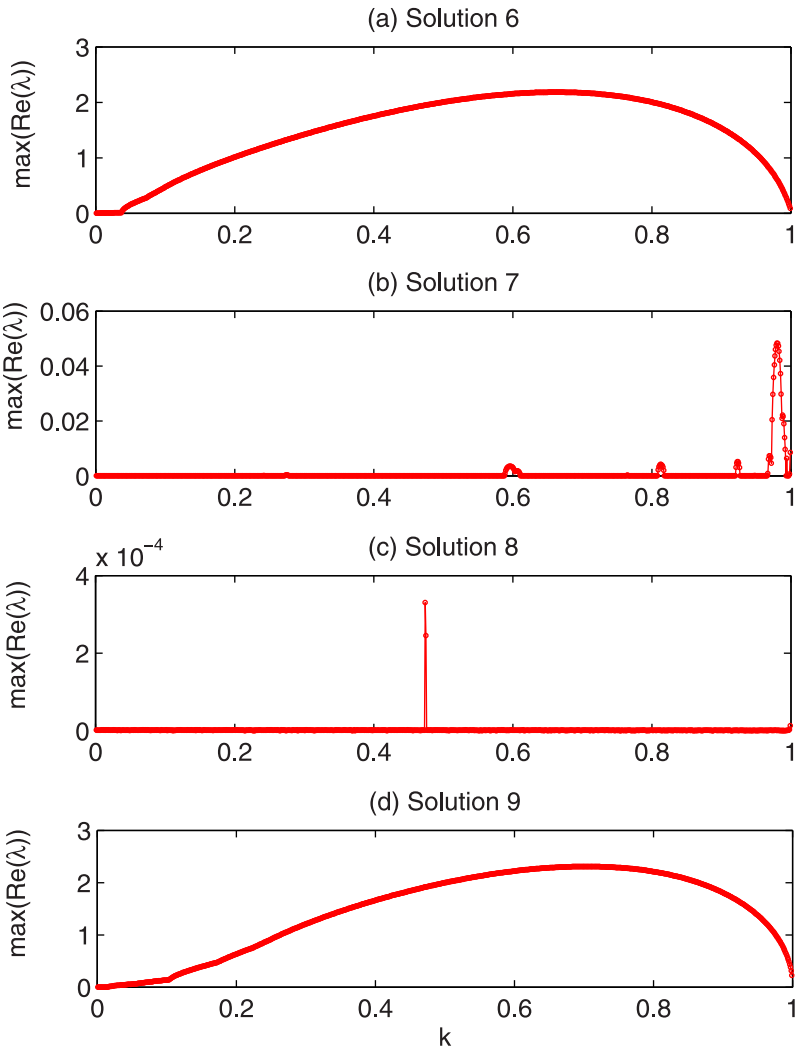

Fig. 9. Maximal real parts of the linear eigenvalues versus the elliptic modulus k for the stationary solutions 6–9 in Eq. (10)–(13) with parameters $a_1 = 1$, $\omega_m = 0 (m = 0, \pm 1)$ and the spin-dependent interaction parameters c_0, c_2 for ^{87}Rb atoms.

condensate, the right column of Fig. 3 indicates that the stationary solution 1 is dynamically unstable for the depth of optical lattice $V_0 = 0.25$, and the left column indicates that it is dynamically stable for $V_0 = 0.75$, which is also consistent with the linear stability analysis in Fig. 1(b).

Figs. 4 and 5 show the linear stability phase diagrams as functions of the depth of optical lattice V_0 and the square of elliptic modulus k^2 for solution 2 and solution 3 in Eqs. (6) and (7), respectively. The other parameters are the same as the parameters in Fig. 1. It is seen from Fig. 4 that in the framework of solution 2 in Eq. (6), the linear stability regions (blue regions) of both ^{23}Na and ^{87}Rb condensates are less than the linear instability regions (red regions); with increasing values of the depth of optical lattice V_0 and the square of elliptic modulus k^2, the linear stability regions of both ^{23}Na and ^{87}Rb condensates become narrower and narrower. It is found from Fig. 5 that the linear stability regions of solution 3 are larger than that of the solutions 1 and 2. In fact, the dn-dn-dn stationary solution 3 in Eq. (7) is the most stable among the nine stationary solutions in Eqs. (5)–(13). In addition, with the same parameters, the linear stability regions of ^{23}Na condensate are larger than that of the ^{87}Rb condensate. The results of dynamical stability analysis for solution 2 and solution 3 in Eqs. (6) and (7) are consistent with that of the linear stability analysis in Figs. 4 and 5.

It is remarked that Bronski et al. [23] pointed out that the trivial phase dn(x, k) solution for one-component repulsive BEC in standing waves is dynamically and linearly stable, while the trivial phase sn(x, k) and cn(x, k) solutions are unstable. Moreover, Bronski et al. [24] also found that for the one-component attractive BEC in standing waves the trivial phase dn(x, k) solution is unstable but the trivial phase sn(x, k) and cn(x, k) solutions have stability regions. In our case, we consider the trivial phase stationary solutions of two types of spinor $F = 1$ BEC, namely the ferromagnetic ^{87}Rb condensate and the polar (antiferromagnetic) ^{23}Na condensate, where the spin-dependent interactions are, respectively, attractive and repulsive. It is seen from Figs. 1,–5

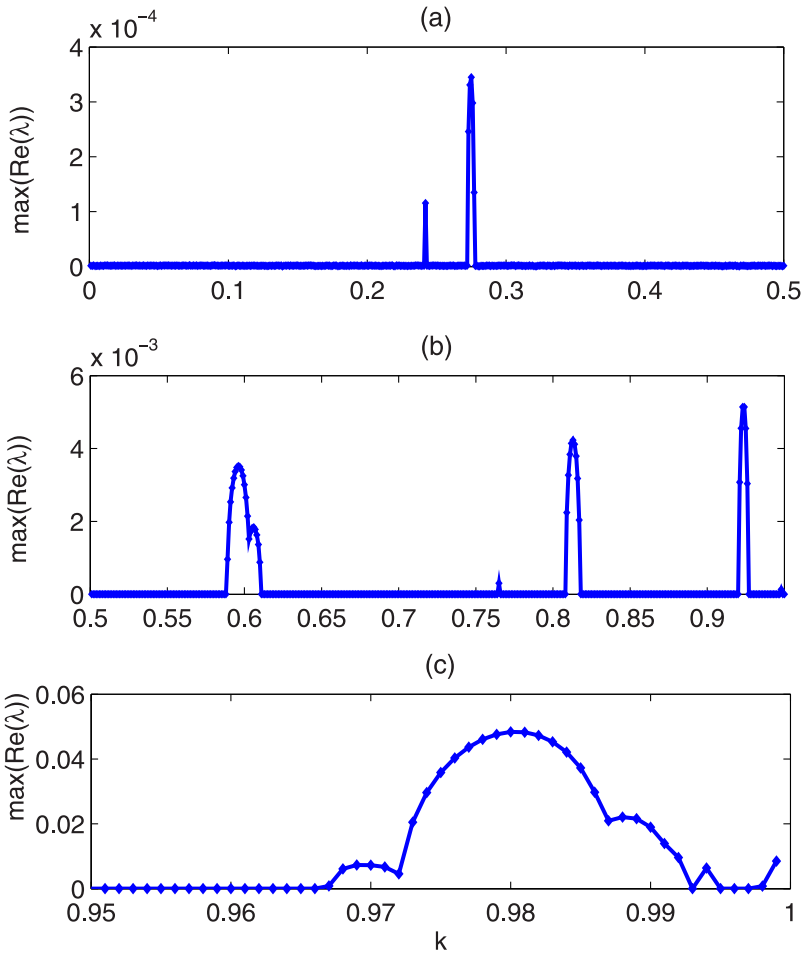

Fig. 10. Maximal real parts of the linear eigenvalues versus the elliptic modulus k for the stationary solutions 7 in Eq. (11) with parameters $a_1 = 1$, $\omega_m = 0 (m = 0, \pm 1)$ and the spin-dependent interaction parameters c_0, c_2 for ^{87}Rb atoms for different k, i.e. $k \in (0, 0.5]$, $k \in [0.5, 0.95]$ and $k \in [0.95, 1)$, respectively.

that the stability regions of the stationary solutions for the spinor $F = 1$ BEC are larger than one-component BEC in [23] and [24]. Moreover, in the spinor $F = 1$ BEC, the three components form stable coexistence states [34] composed of Jacobian elliptic functions.

3.2. Stability of the stationary solutions 4–5

The exact stationary solutions 4–5 in Eqs. (8)–(9) solve the quasi-one-dimensional three component GP Eqs. (2) only when the spin-dependent interaction parameter $c_2 > 0$ and $V_0 = k^2(c_2 - c_0)/(2c_2)$, so they can only describe the dynamics and quantum properties of the polar condensate like ^{23}Na atom. Fig. 6 depicts the real parts of maximal linear eigenvalues versus the elliptic modulus k for the stationary solution 4 in Eq. (8). The spin-dependent interaction parameters c_0 and c_2 are chosen from ^{23}Na atoms and the other parameters are $\omega_1 = \omega_0 = \omega_{-1} = 0$, $a_1 = 1$. It is observed that the stationary solution 4 in Eq. (8) is linearly stable only when the elliptic modulus k sufficiently approaches 0 (see Fig. 6(a)), and for most of the elliptic modulus k it is linearly unstable (see Fig. 6(b)). Figs. 7 and 8 display the time evolutions of the density distributions $|\psi_m|^2 (m = 0, \pm 1)$ and phases of the ^{23}Na condensate described by the stationary solution 4 in Eq. (8) for elliptic modulus $k = 0.001$ and $k = 0.999$, respectively. It is seen that the stationary solution 4 is dynamical stable for elliptic modulus $k = 0.001$ but is dynamical unstable for elliptic modulus $k = 0.999$, which consistent with the result of linear stability analysis in Fig. 6. In the same way, numerical simulations show that the exact stationary solutions 5 in Eq. (9) is both linearly and dynamically unstable.

3.3. Stability of the stationary solutions 6–9

Finally, we analyze the stability of the stationary solutions 6–9 in (10)–(13) numerically. These stationary solutions solve the quasi-one-dimensional three component GP equations (2) only when $c_2 < 0$ and $V_0 = k^2(c_2 - c_0)/(2c_2)$, so they can describe the dynamics and quantum properties of ferromagnetic condensate like ^{87}Rb condensate. Fig. 9(a)–(d) show the maximal real

parts of the linear eigenvalues versus the elliptic modulus k for the stationary solutions 6–9 in Eq. (10)–(13), respectively. It is shown that the stationary solutions 6 and 9 are linearly unstable for most elliptic modulus k, but the stationary solutions 7 and 8 are linearly unstable for only certain regions. Fig. 10(a)–(c) are the separate pictures of the maximal real parts of the linear eigenvalues versus the elliptic modulus k for the stationary solutions 7, which gives the location of the instability regions. Dynamical stability analysis for the stationary solutions 6–9 in (10)–(13) displays the same results as linear stability analysis in Figs. 9 and 10.

4. Conclusions

In conclusion, we have derived nine families of stationary solutions of the three-component GP equations arising from spin-1 Bose–Einstein condensates trapped in a standing light wave in a quasi-1D geometry. The stability of these stationary solutions is analyzed by both linear stability analysis and dynamical evolutions. We demonstrate that in the framework of the same stationary solution the stability regions of condensates with antiferromagnetic spin-dependent interactions are larger than that of the condensates with ferromagnetic ones. The stability regions of the stationary solutions for the spinor $F = 1$ BEC in a standing light wave are larger than that in the one-component BEC in the same standing light wave. Our results suggest that such stationary states are experimentally observable and that a sufficiently large number of condensed spin-1 atoms are required to form a stable, periodic condensate. The experimental developments [35] allow us for direct investigation of the present theoretical results.

Acknowledgments

This work was supported by the NKBRSFC under grant Nos. 2011CB921502, 2012CB821305, NSFC under grants Nos. 11271362, 61227902, 11375030, 61378017, 11434015, SKLQOQOD under grant No. KF201403, SPRPCAS under grants No. XDB01020300, Beijing Natural Science Fund Project and Beijing City Board of Education Science and Technology Key Project No. KZ201511232034, Beijing Natural Science Foundation under Grant No. 1153004, Beijing Nova program No. Z131109000413029 and Beijing Finance Funds of Natural Science Program for Excellent Talents No. 2014000026833ZK19. The Key Projects of Scientific and Technological Research in Hebei Province No. ZD2015133.

References

[1] Stamper-Kurn DM, Andrews MR, Chikkatur AP, Inouye S, Miesner HJ, Stenger J, Ketterle W. Phys Rev Lett 1998;80:2027.
[2] Chang MS, Hamley CD, Barrett MD, Sauer JA, Fortier KM, Zhang W, You L, Chapman MS. Phys Rev Lett 2004;92:140403.
[3] Ho TL. Phys Rev Lett 1998;81:742.
[4] Ohmi T, Machida K. J Phys Soc Jpn 1998;67:1822.
[5] Dabrowska-Wuster BJ, Ostrovskaya EA, Alexander TJ, Kivshar YS. Phys Rev A 2007;75:023617.
[6] Szankowski P, Trippenbach M, Infeld E, Rowlands G. Phys Rev Lett 2010;105:125302.
[7] Nistazakis HE, Frantzeskakis DJ, Kevrekidis PG, Malomed BA, Carretero-Gonzalez R. Phys Rev A 2008;77:033612.
[8] Chang MS, Qin Q, Zhang W, You L, Chapman MS. Nat Phys 2005;1:111.
[9] Ieda J, Miyakawa T, Wadati M. Phys Rev Lett 2004;93:194102.
[10] Su SW, Liu IK, Tsai YC, Liu WM, Gou SC. Phys Rev A 2012;86:013639.
[11] Stamper-Kurn DM, Ueda M. Rev Mod Phys 2013;85:1191.
[12] Morsch O, Oberthaler M. Rev Mod Phys 2006;78:179.
[13] Mishmash1 RV, Carr LD. Phys Rev Lett 2009;103:140403.
[14] Mateo AM, Delgado V, Malomed BA. Phys Rev A 2010;82:053606.
[15] Bludov YV, Konotop VV, Salerno M. Phys Rev A 2010;81:053614.
[16] Cerda-Mendez EA, Sarkar D, Krizhanovskii DN, Gavrilov SS, Biermann K, Skolnick MS, Santos PV. Phys Rev Lett 2013;111:146401.
[17] Masuda S, Nakamura K, del Campo A. Phys Rev Lett 2014;113:063003.
[18] Anderson BP, Kasevich MA. Science 1998;282:1686.
[19] Fallani L, De Sarlo L, Lye JE, Modugno M, Saers R, Fort C, Inguscio M. Phys Rev Lett 2004;93:140406.
[20] Cristiani M, Morsch O, Muller JH, Ciampini D, Arimondo E. Phys Rev A 2002;65:063612.
[21] Greiner M, Mandel O, Esslinger T, Hansch TW, Bloch I. Nature 2002;415:6867.
[22] Eiermann B, Anker T, Albiez M, Taglieber M, Treutlein P, Marzlin KP, Oberthaler MK. Phys Rev Lett 2004;92:230401.
[23] Bronski JC, Carr LD, Deconinck B, Kutz JN. Phys Rev Lett 2001a;86:1402.
[24] Bronski JC, Carr LD, Deconinck B, Kutz JN, Promislow K. Phys Rev E 2001b;63:036612.
[25] Deconinck B, Frigyik BA, Kutz JN. Phys Lett A 2001;283:177.
[26] Lü X. Soliton behavior for a generalized mixed nonlinear Schröodinger model with N-fold Darboux transformation. Chaos 2013;23:033137.
[27] Deconinck B, Kutz JN, Patterson MS, Warner BW. J Phys A: math Gen 2003;36:5431.
[28] Bradley RM, Deconinck B, Kutz JN. J Phys A: math Gen 2005;38:1901.
[29] Kostov NA, Enolskii VZ, Gerdjikov VS, Konotop VV, Salerno M. Phys Rev E 2004;70:056617.
[30] Chacón R, Bote D, Carretero-González R. Phys Rev E 2008;78:036215.
[31] Abramowitz M, Stegun IA. Handbook of Mathematical Functions. New York: Dover; 1965.
[32] van Kempen EGM, Kokkelmans SJJMF, Heinzen DJ, Verhaar BJ. Phys Rev Lett 2002;88:093201.
[33] Klausen NN, Bohn JL, Greene CH. Phys Rev A 2001;64:053602.
[34] Song SW, Wang DS, Wang H, Liu WM. Phys Rev A 2012;85:063617.
[35] Bongs K, Burger S, Dettmer S, Hellweg D, Arlt J, Ertmer W, Sengstock K. Phys Rev A 2001;63.031602(R)